Paddy and Water Environment (2024) 22:257–269
https://doi.org/10.1007/s10333-023-00965-3

ARTICLE

Evaluation of surface damage for in-service deteriorated agricultural concrete headworks using 3D point clouds by laser scanning method

Kazuma Shibano[1] · Nadezhda Morozova[1] · Yuji Ito[2] · Yuma Shimamoto[3] · Yuki Tachibana[4] · Kakutaro Suematsu[4] · Atsushi Chiyoda[4] · Hisaya Ito[4] · Tetsuya Suzuki[2]

Received: 20 January 2023 / Revised: 4 November 2023 / Accepted: 11 December 2023 / Published online: 15 February 2024

Abstract
In the agricultural field, concrete headworks is the most important structure for the irrigation system. In recent years, a number of agricultural concrete infrastructures aging for a long-term period have been increasing. For maintenance and management, conventional inspection methods are time-consuming and costly, such as the electromagnetic wave method and elastic wave method. The detection of surface damage is more effective, safe and reliable than before since the laser scanning method provides detailed geometric information about the structure. The fundamental studies on point cloud data have been conducted in the civil engineering fields; nevertheless, the characteristics of point cloud in agricultural infrastructures, such as dam, headworks and canal, have not been discussed. In this study, 3D point clouds are generated for a concrete irrigation structure using the laser scanning method. The characteristics of surface damage which are quantitatively evaluated using point cloud information, geometric information and intensity parameter are investigated. The types of detected damage are efflorescence and cracks. It is investigated whether point clouds generated from a single scan or multiple scans are more effective for highly accurate detection. The characteristics of surface damage are evaluated by geometric features. The distance between the fitted plane and points is calculated by RANSAC algorithm and roughness parameter. The amount of efflorescence is detected by the distance between the fitted plane from RANSAC algorithm and points. The crack is detected by the local plane fitting method. The types of damage are characterized by the intensity parameter which is related to the color, roughness and moisture of the object. The surface damage and condition are evaluated by both geometric information and intensity parameter. These results show the unique parameters of point clouds from laser scanning methods, such as geometric features and intensity parameter, are useful to evaluate the characteristics of surface damage.

Keywords Laser scanning method · Three-dimensional point clouds · Concrete headworks · Surface damage · RANSAC algorithm

Introduction

The accumulated cracking damage mostly appears on the surface of the in-service irrigation structure. It is important to evaluate that for maintaining each facility's gate function for water utilization. Effective inspection and evaluation methods are required due to the long-term serving and the large amount of agro-infrastructure. In this research, the evaluation method for the characteristics of concrete surfaces by laser scanning parameters in service agricultural structure is proposed.

In the civil engineering fields, non-contact sensors have been developed and used to monitor structures. Acoustic-based sensor, an active technique, can detect the surface condition of structures by the reflection of transmitted signals

✉ Kazuma Shibano
kazuma3267@gmail.com

[1] Graduate School of Science and Technology, Niigata University, 8050 2-no-cho, Ikarashi, Nishi-ku, Niigata 950-2181, Japan

[2] Faculty of Agriculture, Niigata University, 8050 2-no-cho, Ikarashi, Nishi-ku, Niigata 950-2181, Japan

[3] Institute of Agriculture, Tokyo University of Agriculture and Technology, 3-5-8 Saiwai-cho, Fuchu-shi, Tokyo 134-0006, Japan

[4] Nihon Suiko Consultant Co., Ltd, 2-50 Higashi-cho, Omiya-ku, Saitama-shi, Saitama 330-0841, Japan

from a target. It is considered to be difficult to introduce in a generalized setting because these devices are limited to a specific objective (Mutlib et al. 2016). The digital camera was used for monitoring large-size structures with image processing as a passive technique of the non-contact sensor (Fukuda et al. 2010). The damage detection methods, which are conducted an important role in a monitoring system, have evolved much by image-based sensing and machine learning method (Shimamoto et al. 2020; Dung 2019). In our recent research, the development of damage estimation methods for in-service concrete structures by using elastic wave and X-ray CT methods is conducted (Morozova et al. 2022; Suzuki et al. 2020). Thus, the accumulated damage in the concrete structure appears on the surface part, which is detected by the digital image with UAV (Shibano et al. 2022). In recent years, light detection and ranging (LiDAR) and structure from motion (SfM) techniques (DJI 2022; Zhang and Elaksher 2012) provide high-quality point cloud (Lichti and Jamtsho 2006; Jutzi and Gross 2009).

LiDAR technique has been improved and discussed to generate point cloud and modeling for several decades (Kaartinen et al. 2022). The advantage of the terrestrial laser scanner is higher accuracy than dynamic measurement methods, such as mobile laser scanner (MLS) and airborne laser scanner (ALS) (Guo et al. 2011; Che et al. 2019; Mechelke et al. 2007). The resolution of point cloud is restricted by sampling interval and beamwidth (Lichti and Jamtsho 2006). The fundamental principle and characteristics of point cloud by the laser scanning method were investigated in laboratory experiments and simulations (Pfeifer et al. 2008). The accuracy of intensity parameter was validated by the comparison of different types of rangefinders (Suchocki 2020). The effects of surface irregularities, color and incident angle on intensity parameter were confirmed (Nicodemus 1965; Pesci and Teza 2008). The high accuracy of primitive detection for incomplete point clouds was maintained by a reconstructed optimal strategy (Schnabel et al. 2009). From these fundamental results, the management with three-dimensional point clouds was applied in terms of efficiency and upgrading in the construction fields (Mill et al. 2013). The laser scanning method was used to monitor civil infrastructures in many practical cases, such as Moon et al. (2019) and Chang et al. (2005).

The laser scanning method is different from visual images because of acquiring geometric information and intensity parameter (Stałowska et al. 2022). The purpose of the laser scanning method is mainly divided into deformation monitoring, surface defects detection and moisture detection for the maintenance fields. De Blasiis et al. identified and quantified pavement surface defects using geometric information acquired by a mobile laser scanner (De Blasiss et al. 2020). For arch bridges, the structural faults were detected based on shape parameters obtained by laser scanning data (Sánchez-Rodríguez et al. 2018). Using the intensity parameter for evaluation of the surface, Suchocki et al. detected the moisture condition of building materials through the comparison of color, roughness, and saturation (Suchocki and Katzer 2018). For other structures, surface defects, leaks (Tan et al. 2016) and vegetation were detected by classifying the change of surface (Law et al. 2018; Suchocki et al. 2018; Leronas et al. 2016). In the previous research, the effects of moisture condition on the surface of construction material were considered adequately. The laser reflection affected by water should be taken into account in treating the agricultural structure. Therefore, the possible area to measure and the difference in ranging accuracy should be recognized (Lichti 2007).

In this study, evaluation of surface damage is conducted by the laser scanning parameters, geometric information and intensity parameter, revealing the advantages and limitations of each parameter. Deteriorated concrete headworks are selected as a testing structure for a 3D model constructed by the terrestrial laser scanning method. Several point cloud processing, primitive detection (Hackel et al. 2017), RANSAC algorithm, local geometric feature (Weinmann 2013; Jérôme et al. 2011) and intensity analysis (Höfle and Pfeifer 2007) are implemented to evaluate the characteristics of surface damage.

Materials and methods

Monitoring structure

The laser scanning measurement was conducted on in-service deteriorated concrete headworks in Niigata, Japan, which was constructed in 1976 in Fig. 1a. Concrete headworks are one of the main agricultural infrastructures to intake water for irrigation. For the monitoring structure, the span length is approximately 15.0 m and the height is 7.9 m. Surface damage has accumulated due to the long operation period. Cracking situations, efflorescence and surface defects are concentrated in the left side gate pillar in Fig. 1b. This surface is used for the evaluation of this research paper.

Laser scanning method

Laser scanning was conducted to take point clouds of the structure with a FARO® Focus S150 laser scanner in Fig. 2. The international standard on instruments and measurement procedure was developed based on ISO Optics and optical instruments—field procedures for testing geodetic and surveying instruments—2022. The measurement was conducted following ISO 17123: Optics and optical instruments—field procedures for testing geodetic and surveying instruments. The measurement of the laser scanner is performed according

(a) Overview of monitoring structure.

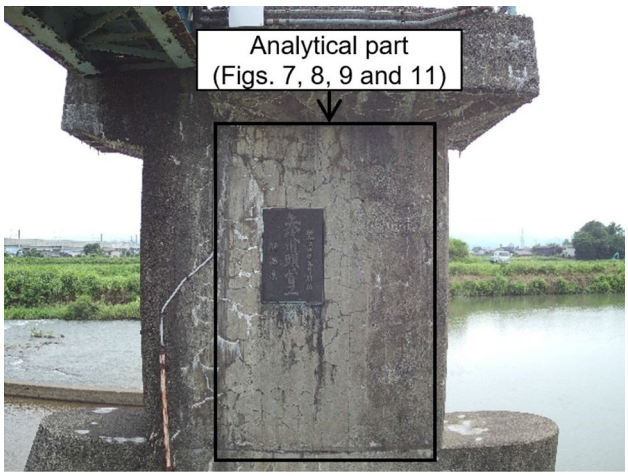

(b) Surface damage condition at left side gate pillar.

Fig. 1 Testing concrete headworks. Overview of monitoring structure e (**a**), surface damage condition at left side gate pillar (**b**)

to this procedure. An infrared laser beam is transmitted into the center of a rotating mirror. The mirror deflects the laser beams vertically with rotation. The scanner detects scattered light that is deflected from surrounding objects. The x, y, z coordinates of each point are then calculated by using angle encoders, which measure the mirror rotation and the horizontal rotation of the scanner. These angles are encoded with the distance measurement. The type of rangefinder is a phase-shift method in Fig. 3.

The relationship between the phase shift in the wave of the infrared light and distances R is shown in the following equation (Eq. 1).

$$R = \frac{\mathrm{ct}}{2},\ t = \frac{\theta}{2\pi f}, \tag{1}$$

Here, c is the speed of light, t is the time, θ is the phase shift, and f is the frequency.

The intensity parameter is registered by the reflectivity of the captured surfaces, measuring the intensity of the received laser beam. The received beam power is described by the following equation (Eq. 2) (Stałowska et al. 2022).

$$P_{\mathrm{R}} = \frac{\pi P_{\mathrm{T}} \rho}{4R^2} \eta_{\mathrm{Atm}} \eta_{\mathrm{Sys}} \cos\alpha \tag{2}$$

where P_{R} is the received signal power, P_{T} is the transmitted signal power, α is the angle of incident, ρ is the reflectance of the material, η_{Atm} and η_{Sys} are the atmospheric and system transmission factors and R is the distance.

Technical specifications of the laser scanner are shown in Table 1. Aligned point clouds were registered using target matching in FARO SCENE software (FARO Technologies 2022). The reference targets were placed to register and merge scans automatically.

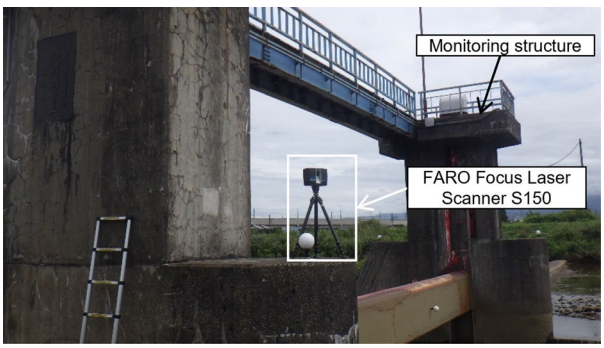

(a) Installing a laser scanner.

(b) FARO Focus Laser Scanner S150.

Fig. 2 Setup for a laser scanner. Installing a laser scanner (**a**) and FARO Focus Laser Scanner S150 (**b**)

Point clouds processing

Point clouds are analyzed using open-source CloudCompare software (Cloudcompare.org 2022a). The analysis surface for evaluation is set in the left side gate pillar surface because of the variety of surface conditions. For complete point clouds of structures, several laser scannings are needed to be conducted from multiple angles. Obtained each point clouds are aligned to get point clouds of the whole structure. In the aligned point clouds, noise is included because of point clouds generated from multiple scans with different accuracy. That is why, in this research, point clouds derived from a single scan are used for quantitative evaluation, while the aligned point clouds are displayed for primitive consideration of the characteristics of point clouds. The noisy data influence result of post-processing consequently (Rusu et al. 2008). The noise is removed by Statistical Outlier Removal (SOR) filter before the post-processing and evaluation (Eq. 3).

$$D_{\max} = D_{\text{ave}} + n\text{Sigma} \times sd \tag{3}$$

where $D_{\max}$ is the threshold of distance for the removal, D_{ave} is the average distance between k nearest neighbors, nSigma is the standard deviation multiplier threshold, and sd is the standard deviation. Point clouds derived from a single scan are selected as an analytical part to evaluate the damage. This is because the error derived from the alignment processing is larger than the errors removed by SOR. The selection of whether to use multiple scans or a single scan should be decided according to the objective and target (Kersten et al. 2005).

The characteristics of surface damage are evaluated based on coordinate and intensity parameters. In this study, surface damage is defined as visible cracks and cracks with efflorescence in the surface field of concrete structure. The distance between the fitted plane estimated from the coordinate and point clouds is calculated and used to evaluate the efflorescence and cracks quantitatively. The motivation for this approach is enabled to detect each designed element for man-made structures (Grilli et al. 2017). The fitted plane is calculated from point clouds of the analytical surface by a least-square method based on RMS error for the conventional method (Jérôme et al. 2011). The coordinate of point cloud used as an argument; therefore, the fitting plane is affected by noise, such as incidental equipment and deposits (Weinmann 2013). RANdom SAmple Consensus (RANSAC) algorithm is introduced to improve the conventional fitting method (Schnabel et al. 2007; Gönültaş et al. 2020). RANSAC algorithm has advantages in terms of robustness, generality, low memory consumption and simplicity. The processing of RANSAC algorithm consists of three parts in Fig. 4. First, minimal point sets from any point clouds are selected (Selected point) randomly, and primitive (Fitting line) is estimated (Fig. 4a). A minimal set is the smallest number of points required to decide a primitive uniquely. The larger the minimal point sets are set, the fewer the number of extracted planes is become, since the small planes are ignored. Next, the score of the shape is calculated by counting surrounding points (Optimal fitting point) in the range of threshold (Threshold for good fit) (Fig. 4b). After any iteration, the shape (Optimal fitting line) is selected when the score of the shape is maximum (Fig. 4c). The distance between the selected plane and point clouds is calculated to evaluate the amount of efflorescence quantitatively (Fig. 4d).

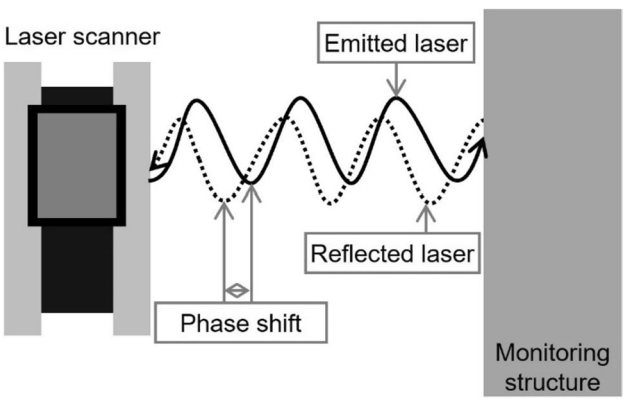

Fig. 3 Phase-shift method

The local geometric features are calculated from the neighbors of points to detect cracks. Many shape signatures were proposed regarding curvature (Douros and Buxton 2002; Teza et al. 2009), normal and local distribution (Dimitrov and Golparvar-Fard 2015). The maximum height of valleys and the maximum height of peaks are defined as roughness according to ISO 25178: geometrical product specifications (GPS)—surface texture: areal (ISO 2021). The distance between points and the best-fitted local plane computed on its nearest neighbors is defined as roughness in the point cloud (Cloudcompare.org 2022b). In this study, roughness is proposed. This value varies depending on the radius defined as the neighborhoods.

In this research, the characteristics of intensity parameter in wet condition are investigated, and then, the characteristics of surface damage are evaluated by geometric and intensity parameters.

Results and discussion

Generation of point clouds

The laser scanning measurement is conducted with the scanner being placed around headworks 20 times to support the completeness of point clouds. The measurement time is less

Table 1 Technical specifications for the FARO® Focus S150 laser scanner and monitoring conditions

Parameter	Condition	Unit	Value
Unambiguity interval (ranging unit)	614 m distance	points/sec	122,000–488,000
	307 m distance		976,000
Range	90% reflectivity (white)	m	0.6–150
	10% reflectivity (dark-gray)		0.6–150
	2% reflectivity (black)		0.6–50
Range noise@10 m distance	90% reflectivity (white)	mm	0.3
	10% reflectivity (dark-gray)		0.4
	2% reflectivity (black)		1.3
Ranging error	–	mm	±1
Field of view (Deflection unit)	–	°	300 vertical/360 horizontal
Wavelength (Laser)	–	nm	1550
Beam divergence (Laser)	–	mrad	0.3
The daily mean temperature	–	℃	23.9
The daily mean humidity	–	%	83
The daily precipitation	–	mm	0.0

than about 30 min per scan. Regarding the weather condition, the daily mean temperature was 23.9°, the daily mean humidity was 83% and the daily precipitation was 0.0 mm as shown in Table 1 (Japan Meteorological Agency 2022). The scanning points are shown in Fig. 5. The number in each circle is in scanning order. Most scanners are located about 10 m from the closest surface. If the surface is scanned at the range of 10 m, the range noise is estimated to be 0.3 mm, 0.4 mm and 1.3 mm at a reflectivity of material of 90% (white), 10% (dark gray) and 2% (black), respectively (see Table 1). Range noise is defined as a standard deviation of values about the best-fit plane for a measurement speed of 122,000 points/sec.

Aligned point clouds are shown in Fig. 6. Analytical result of point clouds is given in Fig. 6a. These point clouds contain constructed elements (e.g., headworks) and unconstructed features (e.g., vegetation and gravel). The point clouds corresponding to headworks are segmented by the clipping box to decrease data volume. The data holes are observed in two areas due to the reflectance characteristics of the object surface and the scanner's constraints. The low-density parts of point clouds around the water are shown in Fig. 6b. A similar phenomenon was observed on point cloud data at the riverbank (Dong et al. 2020). Most of the laser beams are absorbed by the water; therefore, point clouds are not generated. Some laser beams are reflected by water to generate incorrect points as noise (Suchocki and Katzer 2018; Nicodemus 1965). From these results, the detected area of point clouds is affected by the intake season and climate in the case of irrigation facilities. The data holes are observed under the tripods of the scanner in Fig. 6c because of deflection unit specification. The field of view in the vertical direction of this scanner is 300° (see Table 1). The number of neighbors is shown in Fig. 6d. In general, the density

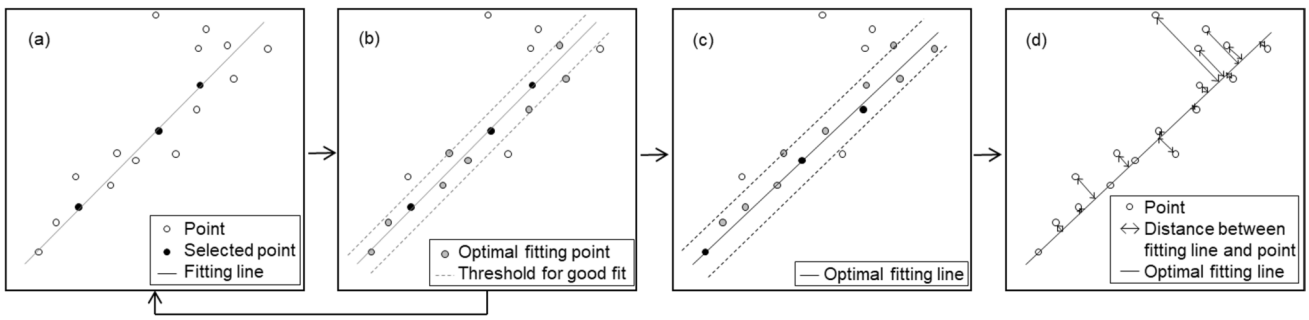

Fig. 4 Evaluation procedure by RANSAC algorithm in 2D. Random sampling and fitting (**a**), calculating scores (**b**), optimal fitting (**c**) and evaluation damage by distance between fitting line and point (**d**)

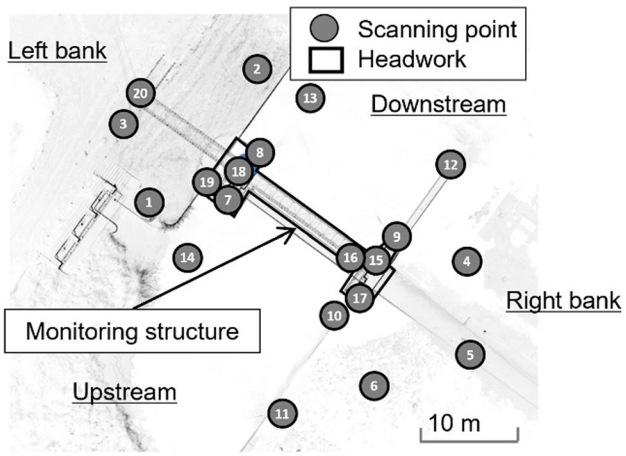

Fig. 5 Scanning points

of point clouds is represented by the number of neighbors within the sphere of any radius *r*. The radius *r* is not decided to be a unique value because it depends on purpose and object. In this analysis, *r* is set to 1.0 cm in order to observe the detailed distribution of density in concrete headwork because of the shape and color of the object surface. The dense parts of point clouds are confirmed at the flat face (e.g., the side face of the left and right piers), while the lower-density parts are confirmed at the corner or edge of the object (e.g., the pipeline and the front side of the weir pillar). Received signals are decreased at low-density parts due to the edge effect. The edge effect refers to the distance averaged by the scanned surface (Stałowska et al. 2022). Point cloud is unable to be acquired without adequate intensity (Soudarissanane et al. 2011). The reasons for varying density are not identified due to relating to many factors (e.g., The number of used scans, distance, scanning time, angle of incident and object characteristics) (Mazalova et al. 2010; Voisin et al. 2007; Costantino and Angelini 2013; Suchocki and Katzer 2018).

Evaluation of cracks and efflorescence by geometric parameters

The point clouds at the left side gate pillar are adapted as the analytical surface in Fig. 7a. Point clouds, shown in Fig. 7, are aligned from the scan data in the previous section. The

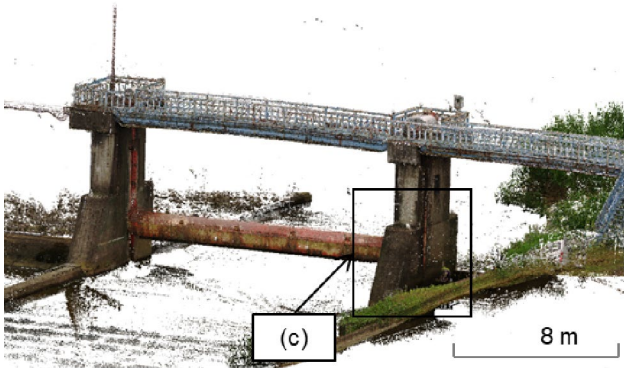

(a) Analytical result of point clouds.

(c) Data hole part (Noise).

(b) The low-density parts of point clouds around the water.

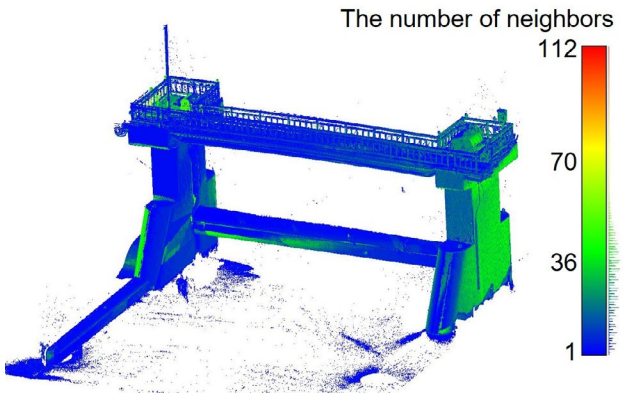

(d) The number of neighbors.

Fig. 6 Generated point clouds. Analytical result of point clouds (**a**), the low-density parts of point clouds around the water (**b**), data hole part (Noise) (**c**) and the number of neighbors (**d**)

(a) Analytical surface at the left side on the left gate pillar.

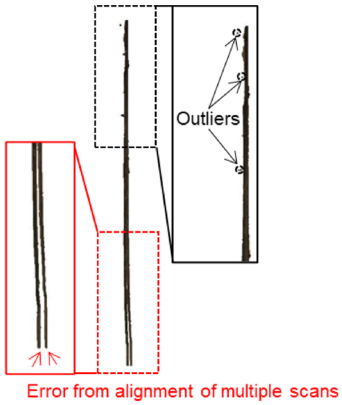

(b) Non-treated point clouds with outliers and multilayers from the side view.

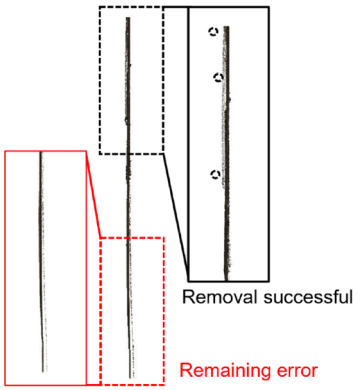

(c) SOR-treated point clouds without isolated points from the side view.

Fig. 7 The result of noise removal processing. Analysis surface at the left side on the left gate pillar (**a**), non-treated point clouds with outliers and multilayers from the side view (**b**) and SOR-treated point clouds without isolated points from the side view (**c**)

side view of Fig. 7a is shown in Fig. 7b, c. The rectangles are shown as enlarged views corresponding to each dotted rectangle. Errors from the alignment of multiple scans are shown in the lower rectangle of Fig. 7b, c. The multiple layer is one of the characteristics of errors by alignment. The outliers are shown in the upper rectangle and circle of Fig. 7b, c. The outliers are point clouds of concrete surface failed ranging. These point clouds, however, include outliers and multilayers since the accuracy of scanning depends on the distance between the scanner and the object surface in Fig. 7b. SOR is performed for whole point clouds in Fig. 7c. Isolated points are removed in the upper rectangle of Fig. 7c, while errors from the alignment of multiple scans remain in the lower rectangle of Fig. 7c. To evaluate geometric features, aligned point clouds are inappropriate. Point clouds generated from a single scan are used in Figs. 8c, d, e, 9 and 11.

Surface damage is evaluated by two plane fitting methods. Examples of plane fitting using full point clouds by conventional method and RANSAC algorithm are depicted in Fig. 8a, b. The whole red plane is detected by the conventional method in Fig. 8a. The color of point clouds depends on each detected surface in Fig. 8b. The different color of planes shows the detected surface corresponding to each face of structural elements. The difference between the two methods is whether they fit a plane locally or globally. It is necessary to process point clouds without noise since the fitted plane is affected by outliers when using the conventional method (Schnabel et al. 2007). The significance of primitive detection is to construct designed structures from unconstructed point clouds (Hackel et al. 2017). In these results, the RANSAC algorithm seems optimal for detecting primitive conceptually. The optimal parameters of RANSAC algorithm are determined from the relationship between the number of detected planes and the detection rate of the target. Optimal minimum support points per primitive are set to seven cases, ten thousand, a hundred thousand and one to five million and investigated. The relationship between the number of detected planes, the detection rate of the analytical surface and the minimum support points per primitive are shown in Table 2. The number of detected planes tends to decrease if the minimum support points per primitive are larger. Detection of the analytical surface failed for the minimum support points per primitive is 4,000,000. In the case that the minimum support points per primitive are lower, the detected planes are likely to be fitted locally and include noise elements (Schnabel et al. 2007). Considering this relationship, the number of minimum support points per primitive is set to 1,000,000 for a single scan according to the balance between detectivity of specific surface and accuracy. The distance between the fitting plane by RANSAC algorithm and points is calculated for the evaluation of the surface condition. The distance between the fitting plane

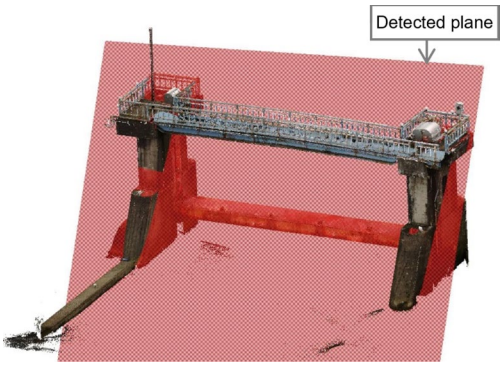

(a) Detected planes by a conventional plane fitting method.

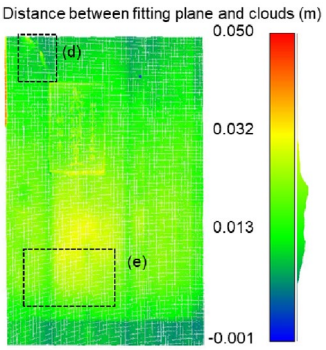

(c) Distance between fitting plane and clouds.

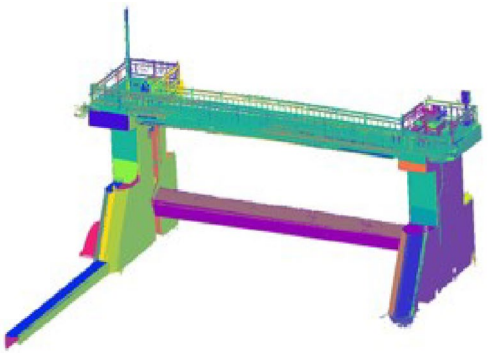

(b) Detected planes by RANSAC algorithm
(The color of the point cloud depends on the detected plane.).

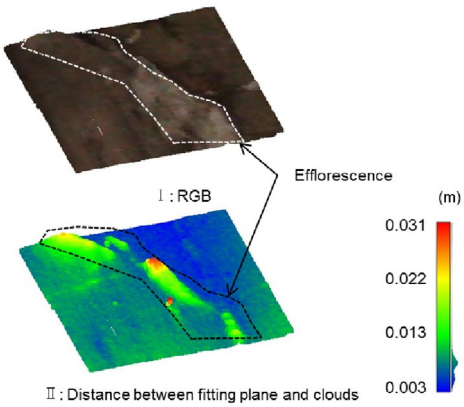

(d) Efflorescence part.

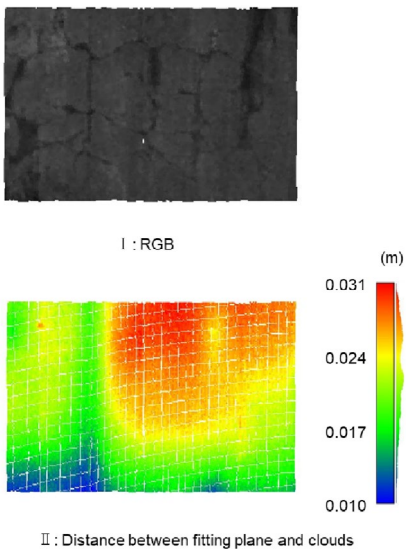

(e) Crack part.

Fig. 8 Detection of damages by primitive detection. Detected planes by conventional plane fitting method (**a**), detected planes by RANSAC algorithm (The color of the point cloud depends on the detected plane.) (**b**), distance between fitting plane and clouds (**c**), efflorescence part (**d**) and crack part (**e**)

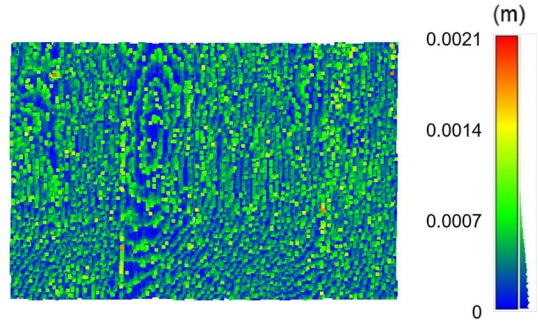

(a) r=0.01 (Rate of concordance=0.604).

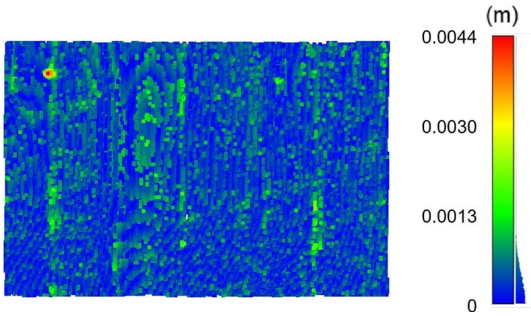

(b) r=0.05 (Rate of concordance=0.643).

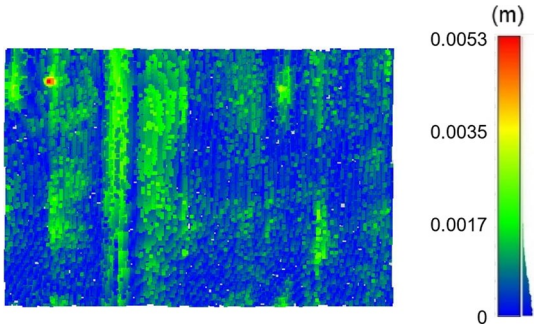

(c) r=0.1 (Rate of concordance=0.630).

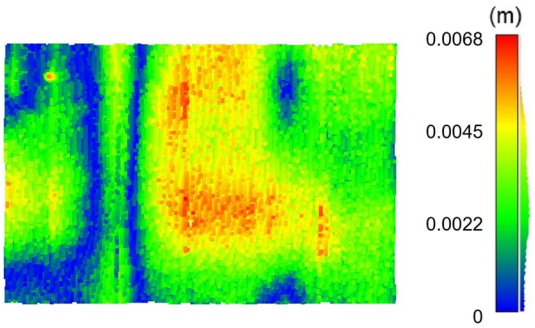

(d) r=0.5 (Rate of concordance=0.532).

Fig. 9 Roughness at crack part. r=0.01 (Rate of concordance=0.604) (**a**), r=0.05 (Rate of concordance=0.643) (**b**), r=0.1 (Rate of concordance=0.630), (**c**) and r=0.5 (Rate of concordance=0.532) (**d**)

and points at the left side gate pillar is shown in Fig. 8c. In the top left part, a larger distance is observed than in the other part ((d) of Fig. 8c). Areas with large distances match the position of efflorescence which is verified by visual inspection in Fig. 8d. The upper and lower figures show RGB point clouds and the distance between the fitting plane and points. Efflorescence indicates the existence of cracks and waterways. The efflorescence part is illustrated by white points in RGB point clouds. The distance between the fitting plane and points at efflorescence is higher than one of the others. The highest point indicates 0.031 m efflorescence is deposited. From these results combined with recognition by image and intensity parameter, efflorescence is able to be quantitatively evaluated by primitive detection and distance between the fitted plane and points. Focusing on the crack part in lower area of analysis surface ((e) of Fig. 8c), crack is not clearly observed by this parameter due to the relative magnitude relationship to efflorescence in Fig. 8e.

The possibilities of local geometric features for crack detection are considered. The asperity of the concrete surface is quantified by geometric features. r is also set to define the neighbors. Roughness which is the local plane fitting method is calculated in Fig. 9. The point clouds shown in Fig. 9 are the same as in Fig. 8e. The optimal r which defines neighbors is chosen from four cases, r=0.01, 0.05, 0.1 and 0.5 m by the rate of concordance to the RGB image. The calculation procedure is mentioned below. The point clouds are converted into an image. Binary images are generated by Otsu method (histogram-based binarization). The rate of concordance for binary images of RGB images and roughness values are calculated, comparing allocated classes. The rate of concordance is 0.604 (r=0.01), 0.643 (r=0.05), 0.630 (r=0.1) and 0.532 (r=0.5). r=0.05 is adopted to calculate roughness. The concordance rate shows a contour matching from the RGB image and inflection line of roughness values. This means the irregular shape of the crack is successfully detected for the average level within the sphere of radius. Therefore, roughness is the most effective parameter to evaluate surface damage in three plane fitting methods.

Detection of surface damage by intensity parameter

Characteristics of intensity parameter need to be revealed since this is affected by measurement environment, laser scanner and material condition. The transmitted signal power, system transmission factor and atmospheric transmission factor related to intensity can be considered constant since scanning is conducted by the same scanner during a short time (Stałowska et al. 2022). Range and angle of incidence are assumed to be the same because of using point clouds generated from a single scan. The reflectivity of a target depends on the roughness, color and saturation of the target surface, especially. In this section, the effects of water, saturation and surface roughness on intensity parameter are focused on. An image of aligned point clouds with RGB and intensity at the bottom part of the weir in wet condition

Table 2 The effects of the minimum support points per primitive on detection of the tested surface by RANSAC

The minimum support points per primitive	The number of detected plane	Detection rate*
10,000	142	+
100,000	39	+
1,000,000	33	+
2,000,000	6	+
3,000,000	4	+
4,000,000	–	–
5,000,000	–	–

*Detection of tested surface: + means successful, – means failed

is shown in Fig. 10a, b and c. Point clouds in wet condition are identified by both RGB and intensity (Fig. 10b, c). The intensity parameter does not dominate over the RGB image for the evaluation of surface damage in wet conditions. Water effects on the reflectance of the laser beam at roughness are based on two phenomena (Suchocki and Katzer 2018). Ordinary, reflection of a laser beam is diffused at a rough concrete surface. A part of an emitted laser beam is absorbed in the interface between water and air. That is why wet concrete surfaces darken and intensity decreases. Environment and weather condition restricts the result of laser scanning.

Visual image and intensity point clouds at the analytical surface are shown in Fig. 11a, b. A lower intensity value (0–200) is allocated at the color change part and nameplate (black), while a higher intensity value (200–241) is allocated at the efflorescence part (white). Intensity values are affected by color (Höfle and Pfeifer 2007). The contour of the crack part is observed by intensity. The intensity value at the crack part is lower than the surroundings. Comparing RGB image, all crack parts are unable to be detected by this method. To reveal the limitation and get a reliable result, the relationship between roughness, intensity and surface condition of the material is analyzed. Tested points are shown by a dotted line in Fig. 11a, b. The relationship between roughness, intensity and surface condition is presented in Fig. 11c. Value deviations on roughness at several parts of efflorescence, framework and cracks are observed. Meanwhile, the detection of cracks with a narrow width is inconclusive. Roughness at the change color part is constant. The intensity value at efflorescence is higher than other parts. The intensity value at the change color part is not constant because of irregular dirt. At the crack part, a decrement in intensity is not observed. Stałowska et al. reported that the maximum crack width detected by geometric information is 2 mm and by intensity is 1 mm at a range of 10 m and an angle of incidence 0 gon (Stałowska et al. 2022). According to this research, a crack whose width is less than 1 mm is impossible to be detected. Crack detection is not simple due to in situ scanning. Intensity shows relative differences depending on surface damage types. The geometric parameter has limitations regarding detecting crack width.

(a) The bottom part of the weir in the wet condition.

(b) Point clouds (RGB).

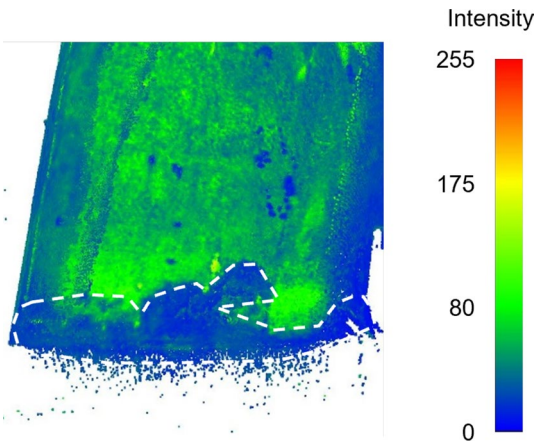

(c) Point clouds (Intensity).

Fig. 10 The characteristics of intensity parameter in wet condition. The bottom part of the weir in the wet condition (**a**), point clouds (RGB) (**b**) and point clouds (Intensity) (**c**)

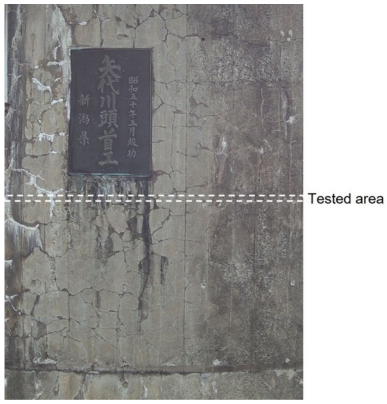

(a) Visual image.

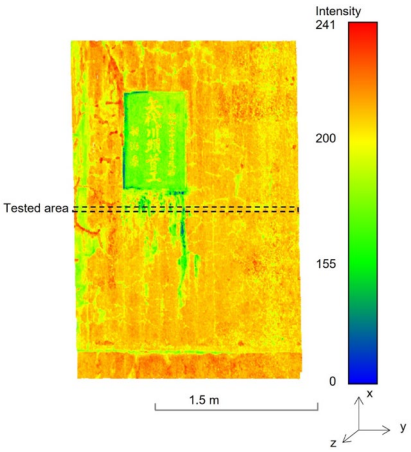

(b) Point clouds (Intensity).

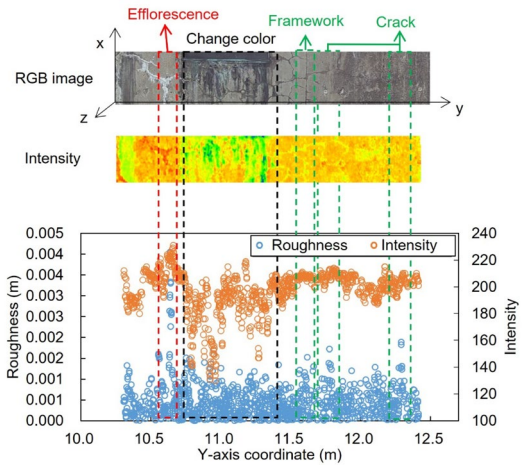

(c) The relationship between roughness and intensity depending on surface condition.

Fig. 11 The evaluation of surface damage types by the intensity and geometric parameters. Visual image (**a**), point clouds (intensity) (**b**) and the relationship between roughness and intensity depending on surface condition (**c**)

The conceptual diagram of evaluation by roughness and intensity depending on the characteristics of the concrete surface is shown in Fig. 12. This relationship is revealed by these results for point clouds derived from a single scan. The roughness and intensity parameters at the efflorescence part are higher than one at the other surface. The roughness of the change color part is constant, while the intensity is lower than others. The roughness at the surface defects part such as a boundary between frameworks and cracks is high values depending on scale, as mentioned. The intensity parameter at the surface defects is lower than one of a non-damaged part. The framework part and crack part have similar characteristics of geometric and intensity parameters. Therefore, the surface damage and condition are characterized by roughness and intensity parameters.

Conclusions

The laser scanning method is applied to evaluate the characteristics of surface damage for agricultural concrete headworks. The evaluation is based on geometric and intensity parameters of point clouds which are generated from laser scanning measurement. Three types of plane fitting methods using coordinate information are attempted for the detection of cracks and efflorescence quantitatively. The characteristics of intensity parameter in wet condition are confirmed. The damage is identified by both geometric and intensity parameters. Conclusions are summarized below:

(1) Point clouds around the water area and under the tripods of the scanner are not detected because of the reflectivity characteristics of water and restraint of the deflection unit.
(2) Aligned point clouds from multiple scans have errors since each scan is measured from a different range. The scale of these errors is larger than the outliers which can be removed by SOR processing. A single scan is used for analytical and evaluation processes.
(3) The amount of efflorescence is evaluated by RANSAC algorithm, while crack parts are not evaluated. The roughness parameter which is calculated from local neighbors enables to detection of cracks quantitatively.
(4) The reliability of intensity parameters in wet condition is lost by the reflectivity of laser beams on water and rough surface. Weather condition and water level affect the limitation of acquiring point clouds and intensity parameter.
(5) The roughness and intensity at the efflorescence part are higher than one of the other parts. The roughness at the crack part is higher than one of the normal parts, while intensity is not changed depending on the crack. The

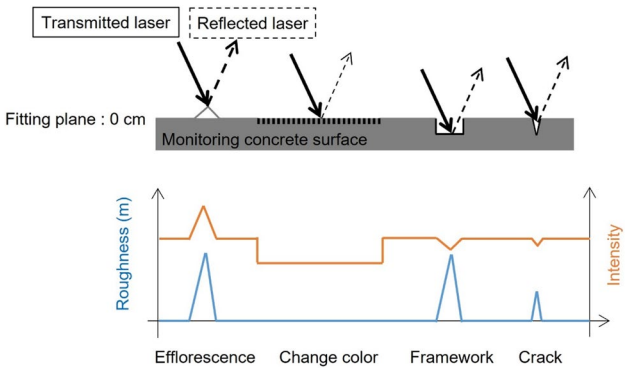

Fig. 12 The conceptual diagram of evaluation by roughness and intensity depending on the characteristics of the concrete surface

variation of intensity increases at change color parts, while roughness is not changed depending on color.

References

Chang KT, Chang JR, Liu JK (2005) Detection of pavement distresses using 3D laser scanning technology. Comput Civ Eng. https://doi.org/10.1061/40794(179)103

Che E, Jung J, Olsen MJ (2019) Object recognition, segmentation, and classification of mobile laser scanning point clouds: a state of the art review. Sensors 19(4):810. https://doi.org/10.3390/s19040810

Cloudcompare.org (2022) CloudCompare—Open Source project. https://www.danielgm.net/cc/. Accessed 2 January 2022

Cloudcompare.org (2022) Roughness https://www.cloudcompare.org/doc/wiki/index.php/Roughness. Accessed 2 January 2022

Costantino D, Angelini MG (2013) Qualitative and quantitative evaluation of the luminance of laser scanner radiation for the classification of materials. In: Proceedings of the ISPRS-International archives of the photogrammetry, remote sensing and spatial information sciences, Strasbourg, pp 2–6. https://doi.org/10.5194/isprsarchives-XL-5-W2-207-2013

De Blasiis MR, Di Benedetto A, Fiani M (2020) Mobile laser scanning data for the evaluation of pavement surface distress. Remote Sens 12(6):942. https://doi.org/10.3390/rs12060942

Dimitrov A, Golparvar-Fard M (2015) Segmentation of building point cloud models including detailed architectural/structural features and MEP systems. Autom Constr 51:32–45. https://doi.org/10.1016/j.autcon.2014.12.015

DJI (2022) Next generation mapping—saving time in construction surveying with drones. https://enterprise.dji.com/news/detail/next-generation-mapping. Accessed 10 December 2022

Dong Z, Liang F, Yang B, Xu Y, Zang Y, Li J, Wang Y, Dai W, Fan H, Hyyppä JU (2020) Registration of large-scale terrestrial laser scanner point clouds: a review and benchmark. ISPRS J Photogramm Remote Sens 163:327–342. https://doi.org/10.1016/j.isprsjprs.2020.03.013

Douros I, Buxton BF (2002) Three-dimensional surface curvature estimation using quadric surface patches. University College London. 44. https://www.academia.edu/15844128/Three_Dimensional_Surface_Curvature_Estimation_using_Quadric_Surface_Patches. Accessed 12 January 2024

Dung CV (2019) Autonomous concrete crack detection using deep fully convolutional neural network. Autom Constr 99:52–58. https://doi.org/10.1016/j.autcon.2018.11.028

FARO Technologies (2022) FARO SCENE software website. https://www.faro.com/en/Products/Software/SCENE-Software. Accessed 2 January 2023

Fukuda Y, Feng MQ, Shinozuka M (2010) Cost-effective vision-based system for monitoring dynamic response of civil engineering structures. Struct Control Health Monit 17(8):918–936. https://doi.org/10.1002/stc.360

Gönültaş F, Atık ME, Duran Z (2020) Extraction of roof planes from different point clouds using RANSAC algorithm. Int J Environ Geoinf 7(2):165–171. https://doi.org/10.30897/ijegeo.715510

Grilli E, Menna F, Remondino F (2017) A review of point clouds segmentation and classification algorithms. Int Arch Photogramm Remote Sens Spat Inf Sci 42:339. https://doi.org/10.5194/isprs-archives-XLII-2-W3-339-2017

Guo L, Chehata N, Mallet C, Boukir S (2011) Relevance of airborne lidar and multispectral image data for urban scene classification using random forests. ISPRS J Photogramm Remote Sens 66(1):56–66. https://doi.org/10.1016/j.isprsjprs.2010.08.007

Hackel T, Wegner JD, Schindler K (2017) Joint classification and contour extraction of large 3D point clouds. ISPRS J Photogramm Remote Sens 130:231–245. https://doi.org/10.1016/j.isprsjprs.2017.05.012

Höfle B, Pfeifer N (2007) Correction of laser scanning intensity data: data and model-driven approaches. ISPRS J Photogramm Remote Sens 62(6):415–433. https://doi.org/10.1016/j.isprsjprs.2007.05.008

ISO (2021) Geometrical product specifications (GPS)—surface texture: areal—Part 2: terms, definitions and surface texture parameters. https://www.iso.org/standard/74591.html. Accessed 2 January 2023

ISO (2022) Optics and optical instruments—field procedures for testing geodetic and surveying instruments. https://www.iso.org/obp/ui/#iso:std:iso:17123:-1:ed-3:v1:en. Accessed 2 January 2023

Japan Meteorological Agency (2022) https://www.data.jma.go.jp/obd/stats/etrn/view/daily_s1.php?prec_no=54&block_no=47612&year=2022&month=9&day=8&view. Accessed 2 January 2023. (in Japanese)

Jérôme D, Clément M, Nicolas D, Bruno V (2011) Dimensionality based scale selection in 3D lider point clouds. ISPRS Int Arch Photogramm Remote Sens Spat Inf Sci 38(5):97–102. https://doi.org/10.5194/isprsarchives-XXXVIII-5-W12-97-2011

Jutzi B, Gross H (2009) Normalization of LiDAR intensity data based on range and surface incidence angle. Int Arch Photogramm Remote Sens Spat Inf Sci 38:213–218

Kaartinen E, Dunphy K, Sadhu A (2022) Lidar-based structural health monitoring: applications in civil infrastructure systems. Sensors 22(12):4610. https://doi.org/10.3390/s22124610

Kersten TP, Sternberg H, Mechelke K (2005) Investigations into the accuracy behaviour of the terrestrial laser scanning system Mensi GS100. Proc 3D Opt Meas Tech 1:122–131

Law DW, Silcock D, Holden L (2018) Terrestrial laser scanner assessment of deteriorating concrete structures. Struct Control Health Monit 25(5):e2156. https://doi.org/10.1002/stc.2156

Leader JC (1979) Analysis and prediction of laser scattering from rough-surface materials. JOSA 69(4):610–628. https://doi.org/10.1364/JOSA.69.000610

Lerones PM, Vélez DO, Rojo FG, Gómez-García-Bermejo J, Casanova EZ (2016) Moisture detection in heritage buildings by 3D laser scanning. Stud Conserv 61:46–54. https://doi.org/10.1179/2047058415Y.0000000017

Lichti DD (2007) Error modelling, calibration and analysis of an AM–CW terrestrial laser scanner system. ISPRS J Photogramm Remote Sens 61(5):307–324. https://doi.org/10.1016/j.isprsjprs.2006.10.004

Lichti DD, Jamtsho S (2006) Angular resolution of terrestrial laser scanners. Photogram Rec 21(114):141–160. https://doi.org/10.1111/j.1477-9730.2006.00367.x

Mazalová J, Valentová K, Vlčková L (2010) Testing of accuracy of reflectorless distance measurement of selected Leica and Topcon total stations. GeoSci Eng 56(1):19–26

Mechelke K, Kersten TP, Lindstaedt M (2007) Comparative investigations into the accuracy behaviour of the new generation of terrestrial laser scanning systems. Proc in the Opt 3:19–327

Mill T, Alt A, Liias R (2013) Combined 3D building surveying techniques–terrestrial laser scanning (TLS) and total station surveying for BIM data management purposes. J Civ Eng Manag 19(1):S23–S32. https://doi.org/10.3846/13923730.2013.795187

Moon D, Chung S, Kwon S, Seo J, Shin J (2019) Comparison and utilization of point cloud generated from photogrammetry and laser scanning: 3D world model for smart heavy equipment planning. Autom Constr 98:322–331. https://doi.org/10.1016/j.autcon.2018.07.020

Morozova N, Shibano K, Shimamoto Y, Tayfur S, Alver N, Suzuki T (2022) Visualization and evaluation of concrete damage in-service headworks by X-ray CT and non-destructive inspection methods. Front Built Environ. https://doi.org/10.3389/fbuil.2022.947759

Mutlib NK, Baharom SB, El-Shafie A, Nuawi MZ (2016) Ultrasonic health monitoring in structural engineering: buildings and bridges. Struct Control Health Monit 23(3):409–422. https://doi.org/10.1002/stc.1800

Nicodemus FE (1965) Directional reflectance and emissivity of an opaque surface. Appl Opt 4(7):767–775. https://doi.org/10.1364/AO.4.000767

Pesci A, Teza G (2008) Effects of surface irregularities on intensity data from laser scanning: an experimental approach. Ann Geophys. https://doi.org/10.4401/AG-4462

Pfeifer N, Höfle B, Briese C, Rutzinger M, Haring A (2008) Analysis of the backscattered energy in terrestrial laser scanning data. Int Arch Photogramm Remote Sens Spat Inf Sci 37:1045–1052

Rusu RB, Marton ZC, Blodow N, Dolha M, Beetz M (2008) Towards 3D point cloud based object maps for household environments. Robot Auton Syst 56(11):927–941. https://doi.org/10.1016/j.robot.2008.08.005

Sánchez-Rodríguez A, Riveiro B, Conde B, Soilán M (2018) Detection of structural faults in piers of masonry arch bridges through automated processing of laser scanning data. Struct Control Health Monit 25(3):e2126. https://doi.org/10.1002/stc.2126

Schnabel R, Wahl R, Klein R (2007) Efficient RANSAC for point-cloud shape detection. Comput Graph Forum 26(2):214–226. https://doi.org/10.1111/j.1467-8659.2007.01016.x

Schnabel R, Degener P, Klein R (2009) Completion and reconstruction with primitive shapes. Comput Graph Forum 28(2):503–512. https://doi.org/10.1111/j.1467-8659.2009.01389.x

Shibano K, Morozova N, Hagiwara T, Shimamoto Y, Suzuki T, Chiyoda A, Suematsu K, Tachibana Y, Ito H (2022) Use of infrared thermography for damage detection of concrete structure by machine learning. In: international workshop on advanced experimental mechanics for students and young researches (IWAEM'22)

Shimamoto Y, Hagiwara T, Suzuki T (2020) Identification of efflorescence in reinforced concrete slab of road bridge by decision tree. Irrig Drain Rural Eng J 88(1):59–65. https://doi.org/10.11408/jsidre.88.I_59. (In Japanese)

Soudarissanane S, Lindenbergh R, Menenti M, Teunissen P (2011) Scanning geometry: Influencing factor on the quality of terrestrial laser scanning points. ISPRS J Photogramm Remote Sens 66(4):389–399. https://doi.org/10.1016/j.isprsjprs.2011.01.005

Stałowska P, Suchocki C, Rutkowska M (2022) Crack detection in building walls based on geometric and radiometric point cloud information. Autom Constr 134:104065. https://doi.org/10.1016/j.autcon.2021.104065

Suchocki C (2020) Comparison of time-of-flight and phase-shift TLS intensity data for the diagnostics measurements of buildings. Materials 13(2):353. https://doi.org/10.3390/ma13020353

Suchocki C, Katzer J (2018) Terrestrial laser scanning harnessed for moisture detection in building materials–Problems and limitations. Autom Constr 94:127–134. https://doi.org/10.1016/j.autcon.2018.06.010

Suchocki C, Katzer J, Rapiński J (2018) Terrestrial laser scanner as a tool for assessment of saturation and moisture movement in building materials. Period Polytech Civ Eng 62(3):694–699. https://doi.org/10.3311/PPci.11406

Suzuki T, Nishimura S, Shimamoto Y, Shiotani T, Ohtsu M (2020) Damage estimation of concrete canal due to freeze and thawed effects by acoustic emission and X-ray CT methods. Constr Build Mater 245:118343. https://doi.org/10.1016/j.conbuildmat.2020.118343

Tan K, Cheng X, Ju Q, Wu S (2016) Correction of mobile TLS intensity data for water leakage spots detection in metro tunnels. IEEE Geosci Remote Sens Lett 13(11):1711–1715. https://doi.org/10.1109/LGRS.2016.2605158

Teza G, Galgaro A, Moro F (2009) Contactless recognition of concrete surface damage from laser scanning and curvature computation. NDT E Int 42(4):240–249. https://doi.org/10.1016/j.ndteint.2008.10.009

Voisin S, Foufou S, Truchetet F, Page DL, Abidi MA (2007) Study of ambient light influence for three-dimensional scanners based on structured light. Opt Eng 46(3):030502. https://doi.org/10.1117/1.2717126

Weinmann M (2013) Feature relevance assessment for the semantic interpretation of 3D point cloud data. ISPRS Ann Photogramm Remote Sens Spat Inf Sci 2:313–318

Zhang C, Elaksher A (2012) An unmanned aerial vehicle-based imaging system for 3D measurement of unpaved road surface distresses. Comput Aided Civ Infrastruct Eng 27(2):118–129. https://doi.org/10.1111/j.1467-8667.2011.00727.x